Direct Numerical Simulations of Laboratory-Scale Stratified Turbulence

Michael L. Waite[1]

Abstract. Turbulence in density-stratified fluids, or stratified turbulence, is an idealized model for the atmospheric mesoscale and oceanic sub-mesoscale. It has been the subject of a number of modelling studies – both laboratory and computational – which have sought to explore the energy cascades of geophysical turbulence. However, there are important differences between atmospheric and oceanic parameter regimes and those accessible in laboratory experiments and numerical simulation. One major difference is the viscous damping by vertical gradients, which can be significant in stratified turbulence even at large Reynolds numbers. Small vertical dissipation is thought to require large buoyancy Reynolds number $Re_b \equiv Fr_h^2\, Re$, where Fr_h is the horizontal Froude number and Re is the Reynolds number. Geophysical values of Re_b are huge, but laboratory experiments and numerical simulations frequently have $Re_b \sim O(1)$. In this chapter, we review recent work on stratified turbulence that has pointed to differences between geophysical- and laboratory-scale dynamics. We also present direct numerical simulations (DNS) of stratified turbulence in the laboratory parameter regime of $Re_b \sim O(1)$. The turbulence in these simulations is extremely dependent on Fr_h and Re, with some (but not all) of this sensitivity accounted for by Re_b. There is also a strong transfer of energy to small horizontal scales, which varies with Fr_h and Re even at constant Re_b. We speculate that this transfer is due to Kelvin–Helmholtz instabilities of the large-scale layerwise flow. Implications of using laboratory experiments and DNS of stratified turbulence as proxies for the atmospheric mesoscale and oceanic sub-mesoscale are discussed.

1. Introduction

As already discussed in previous chapters, stable density stratification is a fundamental property of atmospheric and oceanic flows. Stratification creates buoyancy forces, which inhibit vertical motions and can have a profound effect on dynamics across a wide range of length scales. This chapter is about turbulence in such fluids, which is commonly called stratified turbulence. Stratified turbulence differs from other types of turbulence, such as isotropic three-dimensional, two-dimensional, and quasi-geostrophic (QG) turbulence, in several important ways. It is characterized by approximately horizontal velocities, thin layers of intense vertical shear, quasi-two-dimensional vortices, and interactions with internal gravity waves [for reviews of stratified turbulence, see *Lin and Pao*, 1979; *Hopfinger*, 1987; *Riley and Lelong*, 2000]. We will make a few common idealizations and consider stratified turbulence that is statistically homogeneous, non-rotating, and not dominated by internal gravity waves. For a recent discussion of rotating–stratified turbulence, see *Bartello* [2010], and for gravity waves, see *Staquet and Sommeria* [2002].

Stratified turbulence has relevance for geophysical flows because, over large regions of the atmosphere and ocean, the Brunt–Väisälä frequency N is much larger than the Coriolis parameter f; typical mid-latitude values of N/f are $O(100)$. As a result, there is a range of length scales in both fluids over which buoyancy forces are thought to dominate the Coriolis effect: this range is between larger scales where both rotation and stratification are important, and smaller scales where both effects are negligible. These scales correspond roughly to the atmospheric mesoscale ($O(100)$ to $O(1)$ km) and oceanic sub-mesoscale ($O(1)$ km to $O(100)$ m). The cascade of energy through this scale range forms a key link in the global energy budget, as it connects large-scale QG turbulence with microscale isotropic turbulence and ultimately dissipation. In the case of the atmosphere, various attempts have been made to explain the observed mesoscale energy spectrum with a stratified turbulence hypothesis, which posits that the essential nonlinear dynamics of the mesoscale regime are captured by stratified turbulence [*Gage*, 1979; *Lilly*, 1983; *Lindborg*, 2006]. While its details have evolved, this hypothesis has motivated much of the research on stratified turbulence over the last 30 years. We will use primarily atmospheric terminology in this chapter (e.g. "mesoscale"), but the stratified turbulence hypothesis has also been advanced to explain the sub-mesoscale cascade in the ocean [*Riley and Lindborg*, 2008].

Since the early experiments of the 1960s and 1970s [reviewed by e.g. *Lin and Pao*, 1979] and the pioneering computations of *Riley et al.* [1981], laboratory experiments and numerical simulations have played important roles in investigating the dynamics of stratified turbulence. But even today, there are major differences between the parameter regimes of the atmosphere and ocean and those accessible numerically and in the laboratory. Stratified turbulence is characterized by the Froude and Reynolds numbers. Distinguishing between horizontal and vertical scales (denoted by subscripts h and v), the Froude numbers are

$$Fr_h \equiv \frac{U}{NL_h}, \quad Fr_v \equiv \frac{U}{NL_v}, \tag{1}$$

where U is the horizontal velocity scale, and L_h and L_v are horizontal and vertical length scales. The Reynolds number is given by

$$Re \equiv \frac{UL_h}{\nu}, \tag{2}$$

where ν is the kinematic viscosity. Stratified turbulence requires small Fr_h (for "stratified") and large Re (for "turbulence"), but the definition of "large Re" depends on the degree of stratification. It has been recognized for some time

[1]Department of Applied Mathematics, University of Waterloo, Waterloo, Ontario, Canada.

that, at large but fixed Re, decreasing Fr_h can suppress turbulence [e.g. *Laval et al.*, 2003; *Riley and deBruynKops*, 2003; *Waite and Bartello*, 2004]. Stronger stratifications therefore require larger Reynolds numbers. Building on the work of *Smyth and Moum* [2000] and *Riley and deBruynKops* [2003], *Brethouwer et al.* [2007] argued that stratified turbulence requires large buoyancy Reynolds number

$$Re_b \equiv Re\, Fr_h^2 \equiv \frac{U^3}{\nu N^2 L_h}, \tag{3}$$

which implies that the criterion for "large" Re increases like Fr_h^{-2} as $Fr_h \to 0$. Flows with $Re_b \lesssim 1$ are strongly damped by vertical viscosity, even if $Re \gg 1$ (see §2.3).

Mesoscale motions in the atmosphere lie well inside the stratified turbulence parameter regime: typical values of $U = 10$ ms^{-1}, $L_h = 100$ km, $N = 10^{-2}$ s^{-1}, and $\nu = 10^{-5}$ m^{2}s^{-1} yield

$$Fr_h = 10^{-2}, \quad Re = 10^{11}, \quad Re_b = 10^7. \tag{4}$$

Geophysical values of Fr_h can be readily obtained in the laboratory and computationally, but realizable values of Re, and hence Re_b, are many orders of magnitude smaller. Contemporary laboratory experiments and direct numerical simulations (DNS) of stratified turbulence can obtain Re as high as $O(10^4)$ [e.g. *Praud et al.*, 2005; *Bartello and Tobias*, 2012]. While this is a large value, it is not necessarily sufficient to yield large Re_b at small Fr_h, especially under decaying conditions. For example, consider the decaying grid turbulence experiments of *Praud et al.* [2005]: a representative experiment has initial Froude and Reynolds numbers of 0.086 and 9000, which give $Re_b = 67$. However, as the turbulence decays, U decreases and L_h increases while N and ν stay fixed. Since $Re_b \propto U^3/L_h$, the buoyancy Reynolds number decreases rapidly and falls to $O(1)$ after only a few turnover times. Indeed, *Brethouwer et al.* [2007] surveyed a number of experimental papers and found them all to have $Re_b \lesssim O(1)$, except for when the stratification was very weak.

Direct numerical simulations face a similar challenge in capturing stratified turbulence with large Re_b, because such flows have a wide scale separation between the energy-containing scale L_h, the Ozmidov scale

$$L_O \equiv 2\pi \left(\frac{\epsilon}{N^3}\right)^{1/2}, \tag{5}$$

and the Kolmogorov scale

$$L_d \equiv 2\pi \left(\frac{\nu^3}{\epsilon}\right)^{1/4}, \tag{6}$$

where ϵ is the kinetic energy dissipation rate (length scales are defined with the factor 2π for consistency with the usual wavenumber definitions). The Ozmidov scale is the scale below which isotropic three-dimensional turbulence occurs [*Lumley*, 1964; *Ozmidov*, 1965], while the L_d is the scale below which three-dimensional turbulence is damped by viscosity. Using the Taylor relation $\epsilon \sim U^3/L_h$, it can be shown that the ratios between these scales are

$$\frac{L_O}{L_h} \sim Fr_h^{3/2}, \quad \frac{L_d}{L_O} \sim \frac{1}{Re_b^{3/4}}, \tag{7}$$

so strong stratification at large Re_b necessitates

$$L_h \gg L_O \gg L_d, \tag{8}$$

[e.g. *Brethouwer et al.*, 2007]. Since DNS requires spatial resolutions of $\Delta x \lesssim L_d$ [e.g. *Moin and Mahesh*, 1998], the computational challenge presented by (8) is quite demanding. As a consequence of this difficulty, numerical studies of stratified turbulence commonly employ hyperviscosity or other ad hoc sub-grid scale models to avoid direct resolution of L_d [e.g. *Herring and Métais*, 1989; *Waite and Bartello*, 2004; *Lindborg*, 2006; *Waite*, 2011]. Nevertheless, a number of recent DNS studies have reached modest Re_b values up to $O(100)$ at small Fr_h [*Kimura and Herring*, 2012; *Bartello and Tobias*, 2012; *Almalkie and deBruynKops*, 2012].

In this chapter, we will review and investigate the dynamics of stratified turbulence with buoyancy Reynolds numbers around unity. This is the regime of laboratory-scale stratified turbulence, though it is often employed, via experiments and simulations, as an idealization of the atmospheric mesoscale and oceanic sub-mesoscale. In keeping with both themes of this book – laboratory and numerical models for atmospheric and oceanic flows – we will use direct numerical simulations to investigate the dynamics of lab-scale turbulence. This chapter is about the laboratory parameter regime, not a particular set of laboratory experiments – the focus will be on the use of theory and idealized simulation to better understand turbulence at these scales. We will begin in §2 with a brief review of stratified turbulence theory, including the different parameter regimes, applications to the atmospheric mesoscale, and how viscous effects become important when $Re_b \sim O(1)$, even when the Reynolds number is large. In §3, new DNS of stratified turbulence are presented, with Re_b in the range of 0.2-2. The dependence of energy spectra, transfer spectra, and related length scales on Fr_h, Re, and Re_b is discussed. Conclusions are given in §4.

2. Background

2.1. Equations and Scale Analysis

The equations of motion for an incompressible stratified fluid subject to the Boussinesq approximation are

$$\frac{\partial \boldsymbol{u}}{\partial t} + \boldsymbol{u}\cdot\boldsymbol{\nabla}\boldsymbol{u} = -\frac{1}{\rho_0}\boldsymbol{\nabla} p + b\hat{\boldsymbol{z}} + \nu\,\nabla^2\boldsymbol{u}, \tag{9}$$

$$\boldsymbol{\nabla}\cdot\boldsymbol{u} = 0, \tag{10}$$

$$\frac{\partial b}{\partial t} + \boldsymbol{u}\cdot\boldsymbol{\nabla} b + N^2\, w = \kappa\,\nabla^2 b, \tag{11}$$

where $\boldsymbol{u} = u\,\hat{\boldsymbol{x}} + v\,\hat{\boldsymbol{y}} + w\,\hat{\boldsymbol{z}}$ is the velocity, b is the buoyancy, and p is the dynamic pressure. The definition of b depends on the fluid in question: it is $g\theta/\theta_0$ in a dry atmosphere and $-g\rho/\rho_0$ in the ocean, where θ and ρ are potential temperature and density perturbations, θ_0 and ρ_0 are constant reference values, and g is gravity. The mass diffusivity κ is assumed to be equal to ν, i.e. unit Schmidt number Sc, but much of the following discussion is also valid for the oceanic regime of $Sc \gg 1$. The Brunt–Väisälä frequency N is defined for the atmosphere as

$$N^2 \equiv \frac{g}{\theta_0}\frac{\mathrm{d}\overline{\theta}}{\mathrm{d}z}, \tag{12}$$

where $\overline{\theta}(z)$ is the basic state potential temperature. Here, N is assumed to be constant.

The equations of motion can be nondimensionalized in different ways depending on whether the underlying flow is vortical or wave-like. The main difference in these approaches is in the time scale, which is characterized by the advection time scale L_h/U for vortical flows and the buoyancy time scale $1/N$ for waves [*Drazin*, 1961; *Riley et al.*, 1981; *Lilly*, 1983]. Using the vortical time scale, the dimensionless equations are [following *Riley and Lelong*, 2000]

$$\frac{\partial \boldsymbol{u}_h'}{\partial t'} + \boldsymbol{u}_h'\cdot\boldsymbol{\nabla}_h'\boldsymbol{u}_h' \;+\; Fr_v^2\, w'\frac{\partial \boldsymbol{u}_h'}{\partial z'} = -\boldsymbol{\nabla}_h' p' + \frac{1}{Re}\left(\nabla_h'^2 + \frac{1}{\alpha^2}\frac{\partial^2}{\partial z'^2}\right)\boldsymbol{u}_h', \tag{13}$$

$$Fr_h^2 \left(\frac{\partial w'}{\partial t'} + \boldsymbol{u}_h' \cdot \boldsymbol{\nabla}_h' w' \right) + Fr_v^2 w' \frac{\partial w'}{\partial z'} = -\frac{\partial p'}{\partial z'} + b' + \frac{Fr_h^2}{Re} \left(\nabla_h'^2 + \frac{1}{\alpha^2} \frac{\partial^2}{\partial z'^2} \right) w' \quad (14)$$

$$\boldsymbol{\nabla}_h' \cdot \boldsymbol{u}_h' + Fr_v^2 \frac{\partial w'}{\partial z'} = 0, \quad (15)$$

$$\frac{\partial b'}{\partial t'} + \boldsymbol{u}_h' \cdot \boldsymbol{\nabla}_h' b' + Fr_v^2 w' \frac{\partial b'}{\partial z'} + w' = \frac{1}{Re} \left(\nabla_h'^2 + \frac{1}{\alpha^2} \frac{\partial^2}{\partial z'^2} \right) b', \quad (16)$$

where primes denote dimensionless variables and subscript h denotes horizontal component. The aspect ratio of the flow is

$$\alpha \equiv \frac{L_v}{L_h} \equiv \frac{Fr_h}{Fr_v}. \quad (17)$$

Consider first the inviscid dynamics of (13-16) (viscous effects will be reviewed in §2.3). By definition, strong stratification means $Fr_h \ll 1$. But the limiting behavior of (13-16) is largely controlled by the size of Fr_v, which has so far not been specified. Early work on stratified turbulence was based on the premise of small Fr_v [*Riley et al.*, 1981; *Lilly*, 1983], which leads to the neglect of several terms in (13-16). This assumption implies that vertical advection is small, the flow is nearly in hydrostatic balance, and the horizontal velocity field is approximately non-divergent. The equations of motion reduce to vertically decoupled layers of two-dimensional turbulence in this limit, which is commonly referred to as quasi-two-dimensional, layerwise two-dimensional, or pancake turbulence. More rigorous approaches, based on averaging over high-frequency internal gravity waves, yield the same limiting equations (with the possible inclusion of advection by a vertically sheared horizontal mean flow) [*Babin et al.*, 1997; *Embid and Majda*, 1998].

There is a self-destructive paradox built into the layerwise two-dimensional turbulence picture, which was actually anticipated by *Lilly* [1983] himself. Vertical decoupling implies a collapse of vertical scale. Depending on the ultimate size of L_v after this collapse, the vertical Froude number may no longer be small and the scaling may break down. In the inviscid case, *Lilly* [1983] predicted that Kelvin–Helmholtz instabilities would ultimately develop, halting the vertical collapse and three-dimensionalizing the flow at small scales. Such instabilities were subsequently observed in the numerical simulations of *Laval et al.* [2003] and *Riley and de-BruynKops* [2003], along with a number of subsequent studies.

Billant and Chomaz [2001] revisited the scale analysis of *Riley et al.* [1981] and *Lilly* [1983], and argued that their assumption of $Fr_v \ll 1$ is inappropriate for stratified turbulence. They claimed that the vertical scale would adjust naturally to keep $Fr_v \sim O(1)$, implying that L_v would be set by the buoyancy scale

$$L_b \equiv 2\pi \frac{U}{N}. \quad (18)$$

Note that L_b it is sometimes called the overturning scale because of its association with the appearance of small-scale density overturning [e.g. *Munk*, 1981; *Waite and Bartello*, 2006], and it is distinct from the smaller Ozmidov scale (which, confusingly, is sometimes also called the buoyancy scale). The argument of *Billant and Chomaz* [2001] was based on the self-similarity of the equations of motion when $L_v \sim L_b$, as well as the finding that L_b is the dominant vertical scale of the zigzag instability [*Billant and Chomaz*, 2000]. However, this scaling is also implied by *Lilly* [1983], since L_b is the vertical scale at which the Richardson number of layerwise two-dimensional turbulence becomes $O(1)$ and, presumably, Kelvin–Helmholtz instabilities develop. *Waite and Bartello* [2004] measured L_v in numerical simulations of stratified turbulence and confirmed that $L_v \sim L_b$, and subsequent numerical studies have been consistent with this finding. The inviscid limiting dynamics of (13-16) at $Fr_h \ll 1$ and $Fr_v \sim 1$ are very different from the classical picture of layerwise two-dimensional turbulence. Such turbulence is three-dimensional in the sense that horizontal and vertical advection have the same order of magnitude, but it is anisotropic because $\alpha \sim Fr_h \ll 1$.

2.2. Cascade Theories and Application to the Atmospheric Mesoscale

Observations of the atmospheric kinetic energy spectrum suggest that it has a double power-law form in horizontal wavenumber: at synoptic scales, it has a spectral slope of -3 in agreement with QG turbulence theory [*Charney*, 1971], but in the mesoscale the slope shallows to something resembling -5/3 [*Nastrom and Gage*, 1985; *Cho et al.*, 1999]. A number of different theories were proposed in the late 1970s and early 1980s to explain the observed form of the mesoscale spectrum. *Lilly* [1983] and *Gage and Nastrom* [1986] advanced a stratified turbulence hypothesis: they argued that the layerwise two-dimensional nature of stratified turbulence with small Fr_v might support an inverse cascade of energy through the mesoscale, in analogy with two-dimensional turbulence [*Kraichnan*, 1967]. Such a cascade would require a small-scale source of kinetic energy, which *Lilly* [1983] speculated could be due to moist convection at the $O(1)$ km scale. Around the same time, a different explanation based on a direct cascade of gravity wave energy was proposed [*Dewan*, 1979; *VanZandt*, 1982]. More recent alternatives to the stratified turbulence hypothesis have included theories based on QG and surface-QG turbulence [*Tung and Orlando*, 2003; *Tulloch and Smith*, 2009]. *Waite and Snyder* [2013] have considered the effect of direct mesoscale forcing by latent heating.

Although it was an intriguing idea, the inverse cascade theory for stratified turbulence was not supported by numerical simulations. *Herring and Métais* [1989] attempted to obtain an inverse cascade by applying small-scale forcing in simulations over a range of Froude numbers, but they were unsuccessful. *Lilly et al.* [1998] considered rotating–stratified turbulence with small-scale forcing; they found an inverse cascade when strong rotation was present, but not for purely stratified turbulence. *Smith and Waleffe* [2002] found a direct transfer of energy from small-scale forcing into a vertically sheared mean flow, but there was no cascade through intermediate scales. A theoretical explanation for the lack of an inverse cascade was given by *Waite and Bartello* [2004]: the two-dimensional inverse cascade is a result of the conservation of enstrophy (along with energy) by wavenumber triads; the analogous quantity in stratified turbulence is the potential enstrophy, which is approximately conserved by triads for $Fr_v \ll 1$. But the relationship between energy and (potential) enstrophy is weaker in stratified turbulence than in two-dimensional turbulence, because gravity waves carry some of the energy but no potential enstrophy. Even when $Fr_v \ll 1$, layerwise two-dimensional turbulence eventually leaks energy into gravity waves, which cascade downscale and destroy the possibility of an inverse cascade. More recent data analysis after *Nastrom and Gage* [1985] has also contributed to the rejection of the inverse cascade theory, as it shows a downscale flux of mesoscale energy below scales of around 100 km [*Lindborg and Cho*, 2001].

The lack of an inverse cascade seemed to mark the end of the stratified turbulence hypothesis for the atmospheric

mesoscale, but it was revived in a very different form by *Lindborg* [2006]. The idea that stratified turbulence naturally develops a vertical scale of L_b, and hence $Fr_v \sim O(1)$, suggests that it should be anisotropic but three-dimensional. *Lindborg* [2006] proposed a theory for stratified turbulence with a direct cascade of energy from large to small horizontal scales. Proceeding on dimensional grounds along the lines of the *Kolmogorov* [1941] theory for three-dimensional turbulence, *Lindborg* [2006] argued that the kinetic energy spectrum should have the form

$$E_K(k_h) \sim \epsilon^{2/3} k_h^{-5/3}, \quad E_K(k_v) \sim N^2 k_v^{-3}, \tag{19}$$

in horizontal and vertical wavenumber k_h and k_v. He suggested that the mesoscale kinetic energy spectrum could be understood as a stratified turbulence direct cascade from synoptic scales to the microscale. The same claim has also been advanced by *Riley and Lindborg* [2008] to explain the energy spectrum of the ocean sub-mesoscale.

Lindborg [2006] presented numerical simulations that showed good agreement with (19), at least in the horizontal. To minimize viscous effects and capture the strong anisotropy at small Fr_h, he used thin numerical grids with $\Delta z \ll \Delta x$, along with separate horizontal and vertical hyperviscosity to keep dissipation focused around the grid scale. Most other numerical studies of stratified turbulence have employed isotropic grids with $\Delta z \sim \Delta x$, and have obtained a wider range of spectral slopes. Several DNS studies [*Riley and deBruynKops*, 2003; *Brethouwer et al.*, 2007; *Almalkie and deBruynKops*, 2012; *Bartello and Tobias*, 2012; *Kimura and Herring*, 2012] are broadly consistent with *Lindborg* [2006], despite having much larger dissipation ranges. Steeper spectra, with slopes as low as -5, have been found in some studies [*Laval et al.*, 2003; *Waite and Bartello*, 2004], but as *Brethouwer et al.* [2007] pointed out, this steepening seems to result from excessive vertical dissipation. Horizontal slopes of -2 to -3 have also been found, raising some questions about the universality of (19) [*Waite*, 2011; *Kimura and Herring*, 2012]. The vertical spectrum in (19) has been more difficult to reproduce numerically, but *Kimura and Herring* [2012] have reported a clear -3 slope at small vertical scales. At vertical scales larger than L_b, the vertical spectrum tends to be flat, which is consistent with the layerwise decoupling that occurs for $L_v \gg L_b$ [*Waite and Bartello*, 2004].

Brethouwer et al. [2007] speculated that the stratified turbulence inertial subrange extends down to the Ozmidov scale, below which it transitions to isotropic three-dimensional turbulence. However, the details of this transition are not entirely clear. As envisioned by *Lilly* [1983], the layered structure of stratified turbulence can lead to the development of shear instabilities at small horizontal scales. Such instabilities have been observed in numerical simulations, and are associated with bumps in the kinetic energy spectrum at large k_h [*Laval et al.*, 2003; *Brethouwer et al.*, 2007; *Waite*, 2011]. These bumps are located at horizontal scales around the buoyancy scale, and appear to result from a nonlocal transfer of energy from large, quasi-horizontal vortices to small scale Kelvin–Helmholtz billows [*Waite*, 2011, in simulations that employed hyperviscosity to minimize viscous effects]. These results suggest that L_b rather than L_O marks the small-scale end of the *Lindborg* [2006] inertial subrange. In practice, these scales are usually quite similar, as

$$\frac{L_O}{L_b} \sim Fr_h^{1/2}, \tag{20}$$

so very small Fr_h are required to get a wide separation between L_b and L_O [e.g. *Brethouwer et al.*, 2007].

2.3. Viscous Effects

Our discussion so far has been focused on the inviscid dynamics of (13-16). However, it is viscosity that ultimately distinguishes the laboratory and geophysical regimes of stratified turbulence. *Riley and deBruynKops* [2003] pointed out that viscous coupling rather than Kelvin–Helmholtz instabilities sets the vertical scale of stratified turbulence when viscous effects are sufficiently strong. Assuming a balance between the vertical viscosity and advective terms in (13), they estimated that the resulting vertical scale would be on the order of the viscous scale

$$L_{visc} \equiv 2\pi \sqrt{\frac{L_h \nu}{U}}, \tag{21}$$

(note that L_{visc} is not the same as the Kolmogorov scale L_d). Indeed, numerical simulations have shown strongly layered flows with laminar coupling in the vertical when the stratification is increased at fixed Re (or, analogously, fixed resolution with ad hoc grid-scale dissipation) [*Laval et al.*, 2003; *Waite and Bartello*, 2004]. *Brethouwer et al.* [2007] showed that the vertical scale is set by L_{visc} at small Re_b and L_b at large Re_b, with a transition range over $1 \lesssim Re_b \lesssim 10$. The lab experiments of *Praud et al.* [2005] also exhibit a viscous scaling of vertical scale, consistent with their relatively small values of Re_b.

Viscous effects can be important in strongly stratified turbulence, even at large Reynolds number. When $Re \gg 1$, the horizontal part of the viscous term in (13) is small, but the vertical part has magnitude

$$\frac{1}{Re\,\alpha^2} \sim \begin{cases} 1 & \text{if} \quad Re_b \lesssim 1 \quad (L_v \sim L_{visc}), \\ 1/Re_b & \text{if} \quad Re_b \gtrsim 1 \quad (L_v \sim L_b), \end{cases} \tag{22}$$

[*Brethouwer et al.*, 2007]. So viscous effects due to vertical gradients can be significant at large Reynolds number if the stratification is strong enough to make $Re_b \lesssim 1$. The apparent paradox of strong vertical viscosity at large Reynolds numbers is explained by the anisotropy of stratified turbulence. As stratification increases, the characteristic vertical scale decreases like L_b and the aspect ratio of the flow decreases like Fr_h. At large but fixed Re, L_b ultimately falls inside the vertical dissipation range, at which point the horizontal cascade is suppressed; this transition occurs around $Re_b \sim 1$ [*Riley and deBruynKops*, 2003; *Brethouwer et al.*, 2007]. The cascade theory of *Lindborg* [2006] assumes an inertial subrange in k_h over which viscous effects are negligible, and thus cannot be expected to hold in the laboratory regime of $Re_b \lesssim 1$, where vertical viscosity may not be restricted to large k_h. Instead, simulations point to a steep -5 spectrum when vertical damping (viscous or ad hoc) is strong [*Laval et al.*, 2003; *Waite and Bartello*, 2004; *Brethouwer et al.*, 2007].

3. Direct Numerical Simulation

3.1. Set-Up

In order to further explore the parameter regime of laboratory-scale stratified turbulence, we have performed a number of direct numerical simulations with modest buoyancy Reynolds numbers. Simulations are designed to have roughly equal velocity and length scales, so different Fr_h, Re, and Re_b are obtained by varying N and ν. Three sets of six numerical experiments are considered, corresponding to approximately equal buoyancy Reynolds numbers of ≈ 2, 0.6, and 0.2 (labeled A, B, and C, respectively). In each set of simulations, ν is varied by factors of 1/2 and N is varied by factors of $\sqrt{2}$ to obtain a spread of Re and Fr_h with the same Re_b. The overall ranges of Fr_h and Re are 0.003-0.1 and 200-10 000, respectively, which are realizable values in

Table 1. Parameters, nondimensional numbers, and length scales for each simulation. In the run labels, A, B, C denote runs with approximately equal Re_b; and 1, 2, 3, etc. denote runs with equal ν and approximately equal Re. Dimensional quantities are given in cgs units.

Run	N	ν	n	Δx	Δt	U	L_h	Fr_h	Re	Re_b	L_b	L_o	L_d
A1	0.1	1	128	7.4	0.25	1.6	150	0.11	240	2.7	100	32	16
A2	0.141	0.5	256	3.7	0.125	1.6	170	0.069	530	2.5	71	19	9.4
A3	0.2	0.25	512	1.8	0.0625	1.6	190	0.043	1200	2.3	51	11	5.7
A4	0.283	0.125	512	1.8	0.05	1.6	180	0.032	2400	2.4	37	6.5	3.4
A5	0.4	0.0625	1024	0.92	0.025	1.6	170	0.023	4300	2.3	25	3.8	2.0
A6	0.566	0.03125	1536	0.61	0.0167	1.7	180	0.017	9400	2.6	18	2.4	1.2
B1	0.2	1	128	7.4	0.25	1.6	170	0.046	270	0.58	50	11	16
B2	0.283	0.5	256	3.7	0.125	1.7	180	0.032	620	0.65	38	6.8	9.3
B3	0.4	0.25	512	1.8	0.05	1.7	190	0.022	1300	0.59	26	3.8	5.7
B4	0.566	0.125	512	1.8	0.05	1.7	190	0.016	2500	0.63	19	2.3	3.3
B5	0.8	0.0625	1024	0.92	0.02	1.7	180	0.011	4900	0.63	13	1.4	2.0
B6	1.13	0.03125	1536	0.61	0.0133	1.7	190	0.0081	10000	0.69	9.6	0.87	1.2
C1	0.4	1	128	7.4	0.2	1.7	210	0.020	370	0.15	27	3.9	16
C2	0.566	0.5	256	3.7	0.1	1.8	220	0.014	790	0.16	20	2.4	9.4
C3	0.8	0.25	512	1.8	0.04	1.8	230	0.0097	1600	0.15	14	1.4	5.6
C4	1.13	0.125	512	1.8	0.04	1.8	230	0.0069	3400	0.16	10	0.85	3.3
C5	1.6	0.0625	1024	0.92	0.015	2.0	270	0.0045	8600	0.17	7.7	0.51	1.9
C6	2.26	0.03125	1536	0.61	0.01	1.9	250	0.0034	15000	0.18	5.3	0.31	1.1

laboratory experiments. Parameters for all runs are listed in Table 1.

The computational domain size is $L\times L\times(L/4)$, with periodic boundary conditions on $\boldsymbol{u}$ and b in each direction. The numerical model employs a Fourier-transform-based spectral method with third-order Adams-Bashforth time stepping, and viscous terms are treated implicitly with a trapezoidal approach. The Fourier discretization uses $n \times n \times (n/4)$ wavenumbers, yielding a wavenumber spacing of $\Delta k \equiv 2\pi/L$ in each direction. Aliasing errors are eliminated by the standard 2/3 rule [e.g. *Durran*, 1999], which is implemented by truncating wavevectors $\boldsymbol{k} = (k_x, k_y, k_z)$ outside the sphere

$$|\boldsymbol{k}| \leq \frac{2}{3}\frac{n\pi}{L}. \tag{23}$$

Accounting for this truncation, the effective grid spacing is

$$\Delta x \equiv \Delta y \equiv \Delta z \equiv \frac{3}{2}\frac{L}{n}. \tag{24}$$

The grid spacing for a given ν is chosen to resolve the Kolmogorov scale with $L_d/\Delta x \approx 2$. The time step Δt was selected to be roughly as large as possible while ensuring stability.

Forcing was applied to obtain statistically stationary turbulence and avoid the rapid decay of unforced simulations [as in e.g. *Riley and deBruynKops*, 2003]. We have modified the deterministic forcing approach of *Sullivan et al.* [1994] to excite vortical motion at large horizontal scales [a similar approach was employed by *Bartello*, 2000, to force barotropic vortical motion]. The forcing maintains a fixed value E_0 of horizontally rotational kinetic energy in a cylindrical wavenumber shell with radius k_f, given by

$$|k_h - k_f| \leq \frac{\Delta k}{2}, \quad \text{where} \quad k_h \equiv \sqrt{k_x^2 + k_y^2}. \tag{25}$$

Over every time step, the energy in this shell naturally evolves away from its initial value. The forcing is applied by uniformly scaling the rotational modes in the shell at the end of every time step to return their kinetic energy to E_0. Rotational forcing is used to avoid exciting large-amplitude internal gravity waves at the forcing scale (forcing total kinetic energy was found to produce wave-dominated flows for certain parameter values). Relatively large horizontal scales are forced by setting $k_f = 3\Delta k$.

The dimensional domain size L is set to 2π m for simplicity, so the wavenumber spacing is $\Delta k = 1$ m^{-1}. The forcing level E_0 is chosen to produce velocities comparable to those of laboratory experiments. We let $E_0 = 1$ cm^{2}s^{-2}, which yield rms velocities of $U \approx$ 1-2 cm s^{-1} and dissipation rates of $\epsilon \approx$ 0.02-0.03 cm^{2}s^{-3}. Characteristic horizontal scales calculated from Taylor's relation $L_h \equiv U^3/\epsilon$ are around 2 m, yielding turnover time scales L_h/U of $O(100)$ s. The Kolmogorov scales of the different simulations range between 1-16 cm.

Lower-resolution simulations with $n \leq 512$ are initialized with low-level noise and run for 2000 s. Higher-resolution simulations with $n \geq 1024$ are first spun up to $t = 1000$ s with $n = 512$ and correspondingly lower Re, and then continued to $t = 2000$ s at full resolution. Time series of ϵ (Figure 1) show that the simulations started from rest take several hundred seconds to spin up, while those restarted at $t = 1000$ s adjust much more quickly. The turbulence appears reasonably stationary by $t = 1200$ s in all cases. The various quantities presented below (energy spectra, transfers, etc.) are averaged over the last 800 s of each simulation. Values of Fr_h, Re, and Re_b for each simulation, along with velocity and length scales, are given in Table 1. These values are computed using the rms velocity U, the time-averaged dissipation ϵ, and L_h from Taylor's relation.

3.2. Energy Spectra

Horizontal wavenumber spectra of kinetic energy $E_K(k_h)$ are computed by integrating the energy in each wavevector $\boldsymbol{k}$ over cylindrical wavenumber shells of width Δk [as in e.g. *Waite*, 2011]. In other words, $E_K(k_h)\Delta k$ gives the total kinetic energy in modes with horizontal wavenumbers within $\Delta k/2$ of k_h. Other spectra, such as the potential energy $E_P(k_h)$ and the transfer and buoyancy flux spectra discussed below, are computed similarly.

Over the range of parameters considered here, the kinetic energy spectra are extremely sensitive to Fr_h and Re. Figure 2(a) shows $E_K(k_h)$ from three simulations with the same stratification $Fr_h \approx 0.02$ and different Re. All the spectra are peaked at $k_h/\Delta k = 3$, where kinetic energy is injected by forcing. For the largest Reynolds number (which has $Re = 9400$ and $Re_b = 2.6$), the spectrum exhibits a

short power law range downscale of the forcing with a slope of around -3, followed by a broad spectral bump at larger k_h. As the Reynolds number (and hence Re_b) decreases, the spectrum steepens and the bump is reduced. Similar behavior is displayed in Figure 2(b), which shows spectra from three simulations with the same viscosity and different stratifications. The spectra steepen as the Froude number (and hence Re_b) decreases, while the spectral bump shrinks and moves to higher k_h.

These changes to the kinetic energy spectrum with Fr_h and Re can be partially accounted for by a dependence on Re_b alone [as in *Brethouwer et al.*, 2007]. Spectra from all simulations are plotted Figure 3, where they are arranged into groups of approximately equal values of $Re_b \approx 2$, 0.6, and 0.2. The forcing and power law portions of the spectra collapse fairly well at constant Re_b, at least for k_h not too large. The spectral slopes of the power law range are plotted in Figure 4 (slopes are computed with a least squares fit over $4 \leq k_h/\Delta k \leq 10$; note that for the lowest Re simulations in Figure 3a, there is no clear distinction between the power law range and spectral bump). The changes in slope obtained at constant Re_b are for the most part much smaller than changes at constant Fr_h or Re. All spectra are steeper than -5/3, which as discussed in §2.3 is to be expected at these values of Re_b. Overall, smaller Re_b yield steeper spectra: slopes are around -3, -4, and -5 for $Re_b \approx 2$, 0.6, and 0.2. The collapse is very good for smaller Re_b, where the slopes vary by less than 10% at constant Re_b. A greater spread in slopes is found for $Re_b \approx 2$: in these simulations, there is a clear steepening from around -2 to -3 as Fr_h decreases and Re increases, even though Re_b is approximately constant. The slopes appear to have not quite converged in this case, and may steepen below -3 for even smaller Fr_h and larger Re.

At larger wavenumbers the collapse of the spectra in Figure 3 is not particularly good. For each Re_b, the spectra obtained with the lowest Reynolds numbers have only a short power law range between the forcing and dissipation wavenumbers. However, a spectral bump eventually emerges in each case as Re increases and Fr_h decreases. As Re_b decreases, higher values of Re (and hence smaller Fr_h) are required for a spectral bump to appear: for $Re_b \approx 0.2$, only the two highest-Re cases exhibit a bump downscale of the steep -5 spectrum. The position of the bump appears to move to larger k_h as Re increases and Fr_h decreases, but its shape is quite variable; in general, it is broader for large Re_b, and it narrows (or disappears entirely) as Re_b decreases. These findings are reminiscent of the buoyancy-scale bumps described by *Waite* [2011], which were located at k_h around the buoyancy wavenumber $k_b \equiv 2\pi/L_b \equiv N/U$. The possible relationship between the spectral bumps in Figure 3 and the buoyancy scale is investigated further below.

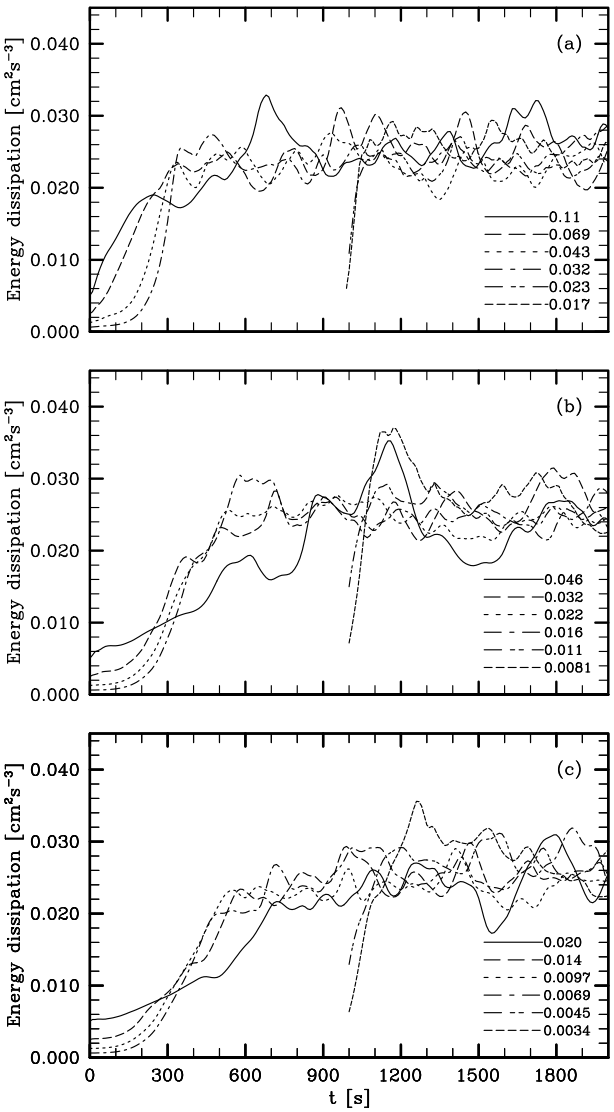

Figure 1. Time series of kinetic energy dissipation in simulations with $Re_b \approx$ (a) 2, (b) 0.6, and (c) 0.2 (simulation sets A, B, and C). Dash patterns denote different Fr_h.

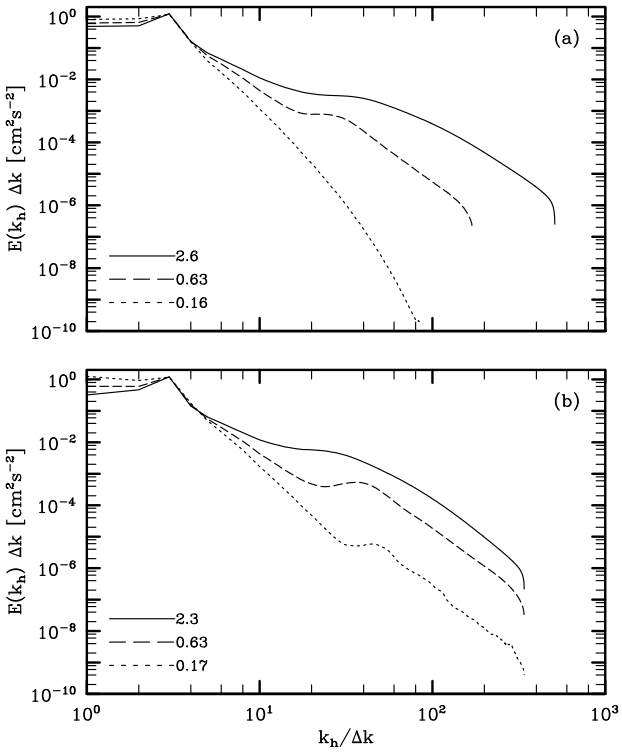

Figure 2. Horizontal wave number spectra of kinetic energy in simulations with (a) fixed $N = 0.566$ s^{-1} and different ν (and hence different Re and Re_b, i.e. runs A6, B4, and C2); and (b) fixed $\nu = 0.0625$ cm^{2}s^{-1} and different N (and hence different Fr_h and Re_b, i.e. runs A5, B5, and C5). Dash patters denote different Re_b.

3.3. Energy Budget

The spectral budget of kinetic and potential energy is governed by the equations

$$\frac{\partial}{\partial t}E_K(k_h) = T_K(k_h) + B(k_h) - D_K(k_h) + F(k_h), \quad (26)$$

$$\frac{\partial}{\partial t}E_P(k_h) = T_P(k_h) - B(k_h) - D_P(k_h). \quad (27)$$

The terms $T_K(k_h)$ and $T_P(k_h)$ are the transfer spectra of kinetic and potential energy, which represent conservative exchanges of energy between different wavenumbers by nonlinear interactions. The $B(k)$ term is the buoyancy flux, which is given by the cross spectrum of vertical velocity and buoyancy; it describes the wavenumber-local conversion of potential to kinetic energy, and so it appears in both equations (26) and (27) with opposite signs. The $F(k_h)$ term denotes injection of kinetic energy by forcing (potential energy is not directly forced in these simulations), while $D_K(k_h)$ and $D_P(k_h)$ are the viscous and diffusive dissipation of kinetic and potential energy. These dissipation terms include the contributions from both horizontal and vertical gradients, and so their effects are not necessarily dominated by large k_h, as in a typical dissipation range at large Re.

Figure 6 shows the transfer and buoyancy flux spectra from three simulations with the same stratification $Fr_h \approx 0.02$ and different Re. Dissipation and forcing terms are not shown, but can be deduced as residuals since the spectra are approximately stationary. For the largest Re (Figure 6a), three distinct spectral ranges are apparent. Small wavenumbers are dominated by the forcing: kinetic energy is injected around $k_h/\Delta k \approx 3$, where it is primarily removed by nonlinear interactions and sent downscale (the rest is dissipated directly at k_f or converted to potential energy). For $k_h \gtrsim k_f$, there is a range over which $T_K(k_h)$ and (to a lesser extent) $T_P(k_h)$ are positive and $B(k_h) \approx 0$. If this range of k_h were a true inertial subrange, the transfer would be zero. The positive transfer implies that some of the kinetic energy injected into these scales is dissipated, which is to be expected since $Re_b = 2.6$ is not very large.

Downscale of this plateau of positive transfer, there is a major transition in the spectral energy balance. A large peak in $T_K(k_h)$ around $k_h/\Delta k \approx 40$ points to a significant injection of kinetic energy. Some of this energy is converted to potential energy via the negative peak in buoyancy flux around the same scale, and the rest is dissipated. As the Reynolds number (and hence Re_b) decreases, strong dissipation is felt over a wider range of k_h, and the small-scale peaks in transfer and buoyancy flux are suppressed (Figures 6b,c). In the smallest Re_b case, the energy injected by forcing is transferred only to nearby wavenumbers, where it is dissipated directly.

Figure 7 shows transfer and buoyancy flux spectra from three simulations with approximately equal buoyancy

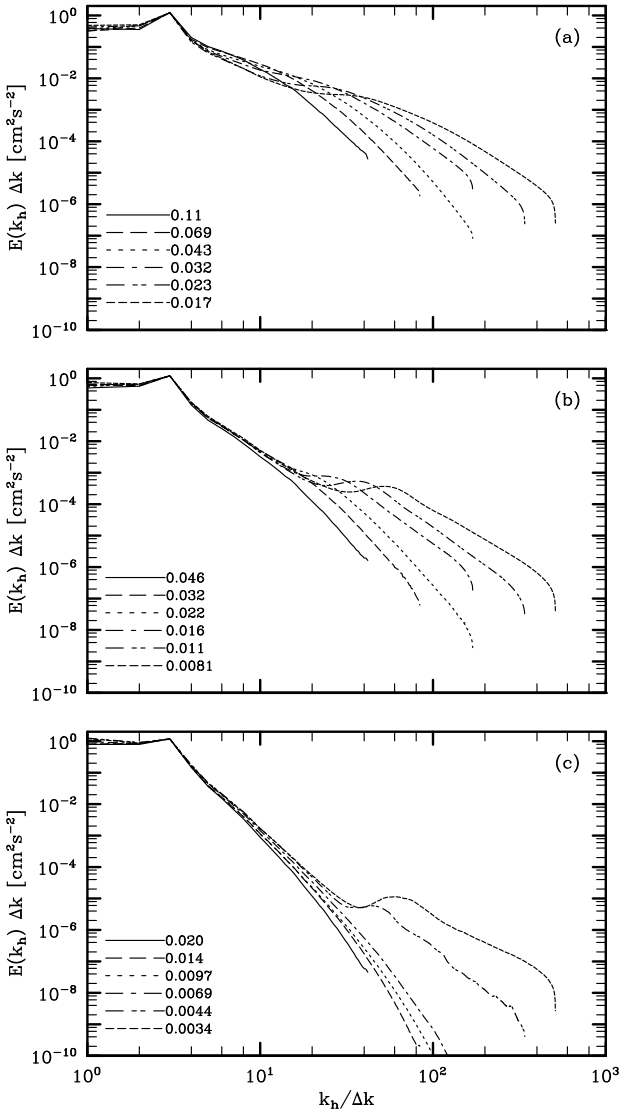

Figure 3. Horizontal wave number spectra of kinetic energy in simulations with $Re_b \approx$ (a) 2, (b) 0.6, and (c) 0.2 (simulation sets A, B, and C). Dash patterns denote different Fr_h.

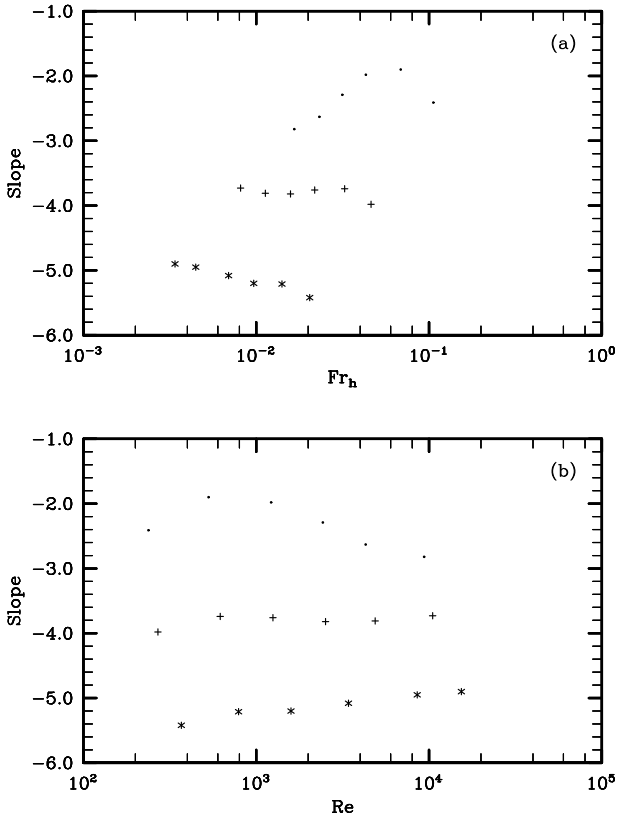

Figure 4. Spectral slopes of the horizontal wave number spectra of kinetic energy, plotted vs. (a) Fr_h and (b) Re for $Re_b \approx 2$ ($\cdot$), 0.6 ($+$), and 0.2 ($*$) (simulation sets A, B, and C).

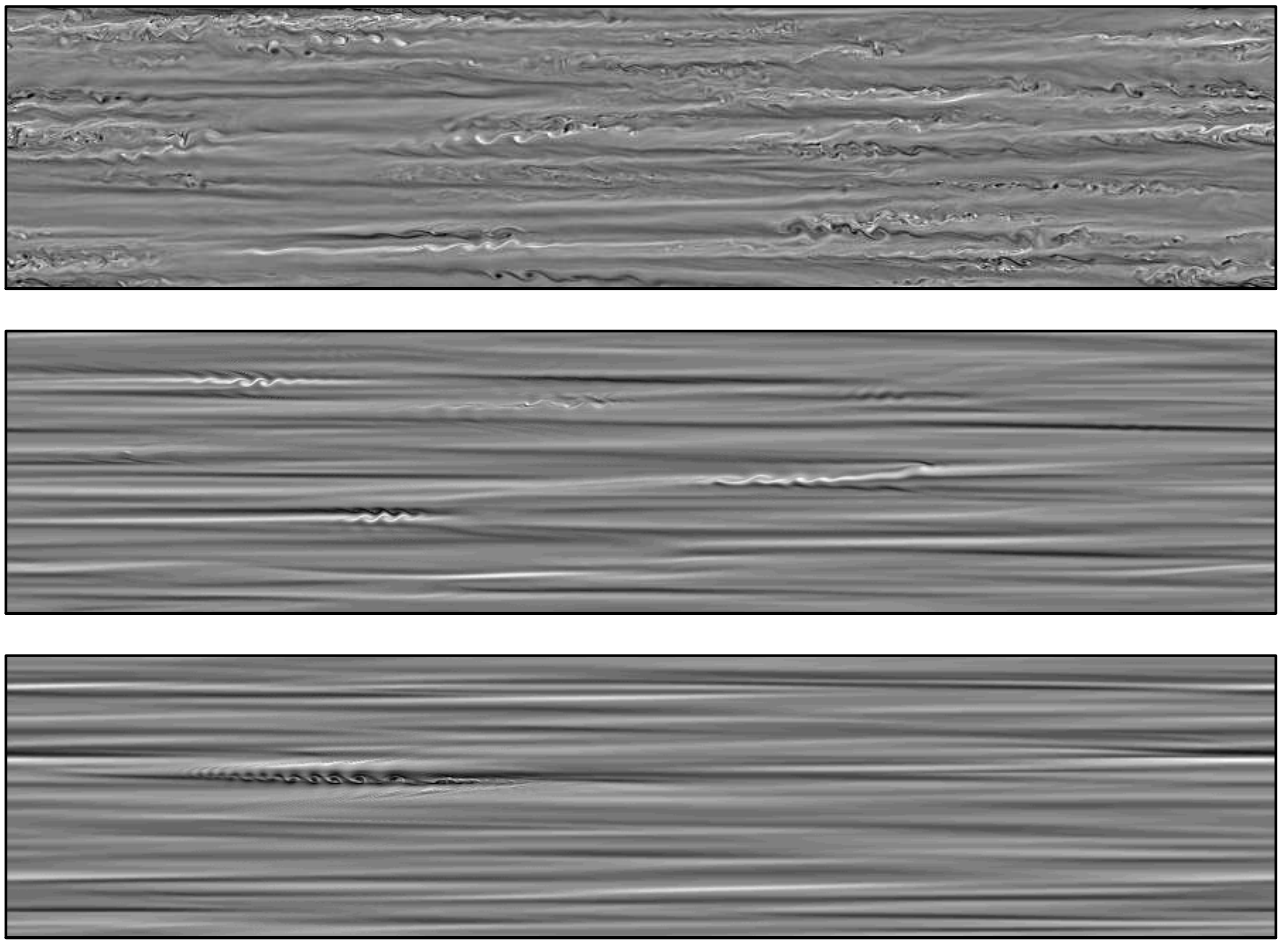

Figure 5. Vertical (x,z) slices of the y-component of vorticity in simulations with fixed $\nu = 0.03125$ cm^{2}s^{-1} and different N (and hence different Fr_h and Re_b), corresponding to $Re_b = 2.6$ (top), 0.69 (middle), and 0.18 (bottom) (runs A6, B6, and C6). Shading is saturated to white/black at ± 3 s^{-1}. Fields in (a) and (b) are plotted at the final time of the simulations $t = 2000$ s. Panel (c) is plotted at $t = 1900$ s, which was chosen to illustrate the lone patch of Kelvin-Helmholtz billows visible at this time.

Reynolds numbers around 2. These spectra are consistent with the picture described above: there is a short forcing range, followed by a plateau of positive transfer and negligible buoyancy flux, followed by large peaks of positive $T_K(k_h)$ and negative $T_P(k_h)$ and $B(k_h)$. As Fr_h decreases and Re increases, the plateau gets longer as the peaks move downscale (in Figure 7a, the peaks are adjacent to the forcing range and no plateau is obtained). The position of the peak moves to larger k_h as Fr_h decreases and Re increases, similar to the spectral bumps in Figure 3(a). The magnitude of the bump does not diminish with decreasing Fr_h, suggesting that even smaller Fr_h with $Re_b \approx 2$ would yield a similar injection of kinetic energy and negative buoyancy flux at even larger k_h.

At the smallest values of $Re_b \approx 0.2$, Figure 6(c) suggests that the transfer becomes very small just downscale of the forcing, where the energy spectra have steep slopes of around -5. This range is magnified with logarithmic axes in Figure 9, which shows transfer and buoyancy flux spectra for two simulations with $Re_b \approx 0.2$. The top panel is representative of the cases when $Fr_h \gtrsim 0.007$. For all $k_h \gtrsim k_f$, the total transfer dominates the buoyancy flux by at least an order of magnitude, and is balanced by the vertical part of the dissipation. It has a spectral slope of around -4 at large scales, but falls off faster than a power law at larger k_h. As observed above for larger Re_b, a small-scale transition emerges in the energy balance at sufficiently small Fr_h and large Re (Figure 9b), where a small bump of positive transfer and negative buoyancy flux emerges at large k_h. These bumps are quite intermittent, appearing and disappearing over the averaging interval $1200 \leq t \leq 2000$ s. In the averaged spectra in Figure 9(b), they are centered around $k_h/\Delta k \approx 60$.

3.4. Length Scales

In physical space, these simulations exhibit the familiar structure seen in a number of recent studies of stratified turbulence: thin layers of predominantly horizontal velocity at large horizontal scales along with, in some cases, shear instabilities and small-scale turbulence [e.g. *Laval et al.*, 2003; *Riley and deBruynKops*, 2003; *Brethouwer et al.*, 2007; *Waite*, 2011; *Bartello and Tobias*, 2012]. Figure 5 shows representative snapshots of the y-component of vorticity, which is dominated by the vertical shear $\partial u/\partial z$, for three different Re_b values (the simulation with the largest Re is shown in each case). For $Re_b = 2.6$, there are several patches resembling Kelvin–Helmholtz instabilities, some of which appear to have transitioned to smaller-scale turbulence. However, much of the domain remains quiet, with a smooth, layerwise structure. As Re_b decreases, the regions of instability become increasingly intermittent and without the associated breakdown into smaller-scale turbulence; at the time of the snapshots in Figure 5, only a few patches of instability are visible for $Re_b = 0.69$, and one for $Re_b = 0.18$.

The vertical scale of the layers seen in Figure 5 can be measured from the first moment of the vertical wavenum-

ber spectrum of kinetic energy $E_K(k_v)$ (which is computed in an analogous fashion to the horizontal spectrum). We define the characteristic vertical scale to be

$$L_v \equiv 2\pi \frac{\int E_K(k_v)\,\mathrm{d}k_v}{\int k_v E_K(k_v)\,\mathrm{d}k_v}, \tag{28}$$

[a similar definition based on the 1/2-moment was used by *Waite and Bartello*, 2004; *Brethouwer et al.*, 2007, used (28)]. As discussed in §2, the vertical scale of stratified turbulence is expected to scale like L_{visc} when the layer thickness is set by viscous coupling, and L_b when the layers break down into shear instabilities and small-scale three-dimensional turbulence. In Figure 10, the vertical scale in all simulations is plotted against L_b and L_{visc}. The buoyancy and viscous scales are similar in these simulations, since (18) and (21) imply that

$$\frac{L_b}{L_{visc}} = \sqrt{Re_b}, \tag{29}$$

and our $\sqrt{Re_b}$ values range from 0.39 to 1.6. Nevertheless, the L_{visc} scaling is more convincing than the L_b scaling. The layer thickness in these simulations therefore seems to be set by viscosity, which is consistent with our relatively small values of Re_b [as in *Brethouwer et al.*, 2007]. Note, however, that (29) can also be interpreted as a vertical Froude number for $L_v \sim L_{visc}$, which is therefore not much smaller than $O(1)$. Since U and L_v are based on mean quantities, we expect our simulations to have patches with locally larger U and smaller L_v, which would therefore be susceptible to instabilities like those visible in Figure 5.

In the horizontal, the spectral bumps described above suggest a definition of a transition length scale. Following

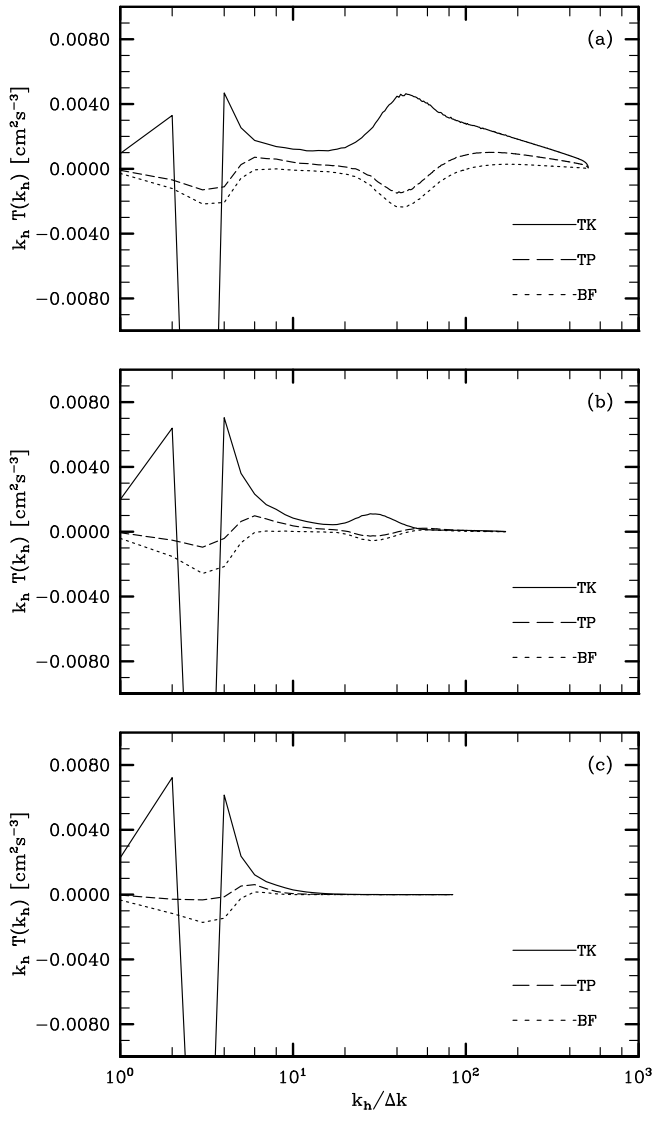

Figure 6. Horizontal wave number spectra of kinetic and potential energy transfer and buoyancy flux in simulations with fixed $N = 0.566$ s^{-1} and different ν (and hence different Re and Re_b), corresponding to $Re_b =$ (a) 2.6, (b) 0.63, and (c) 0.16 (runs A6, B4, and C2, as in Figure 2a). Spectra are multiplied by k_h to preserve area under the curves with log–linear axes.

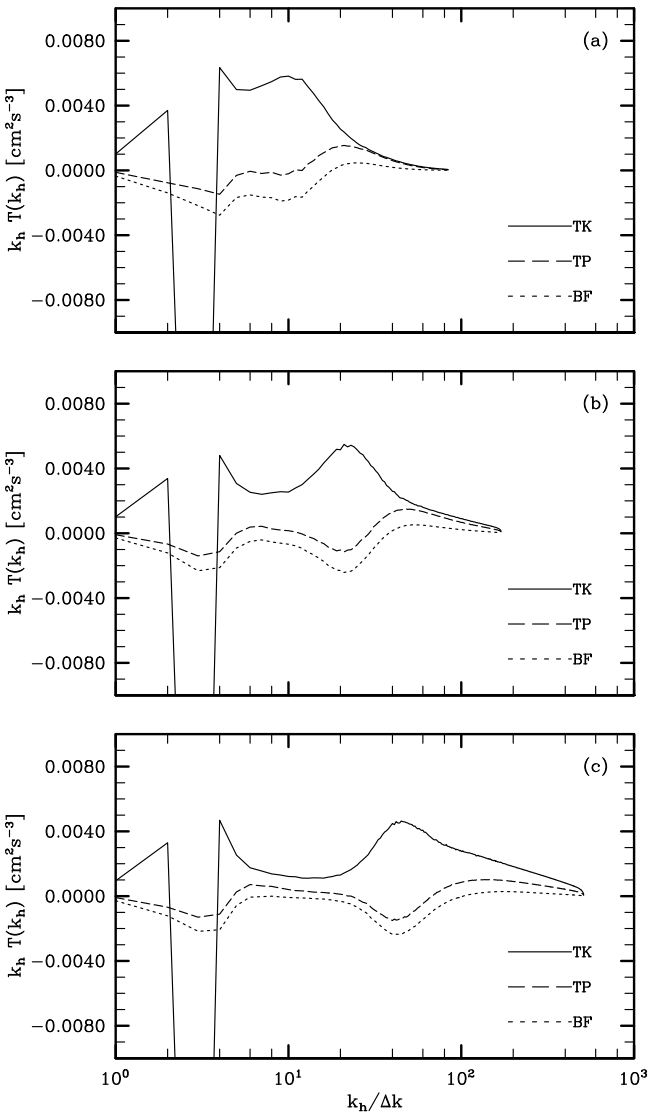

Figure 7. Horizontal wave number spectra of kinetic and potential energy transfer and buoyancy flux in simulations with fixed $Re_b \approx 2$ and different Fr_h and Re, corresponding to $Fr_h =$ (a) 0.069, (b) 0.032, and (c) 0.017 (runs A2, A4, and A6). Spectra are multiplied by k_h to preserve area under the curves with log–linear axes.

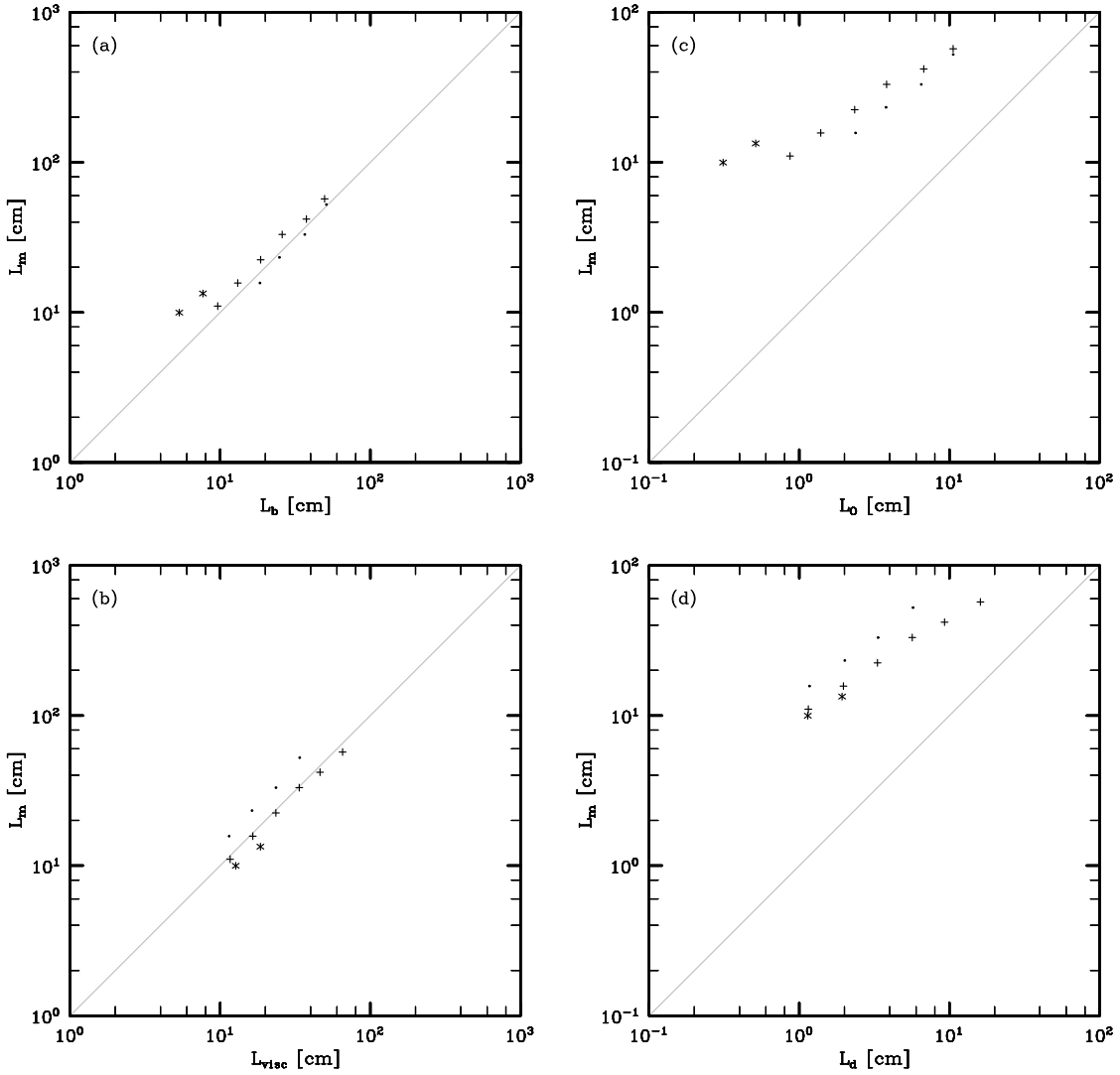

Figure 8. The horizontal scale L_m of minimum small-scale buoyancy flux, plotted against (a) the buoyancy scale L_b, (b) the viscous scale L_{visc}, (c) the Ozmidov scale L_O, and (d) the Kolmogorov scale L_d. Symbols denote $Re_b \approx 2$ ($\cdot$), 0.6 ($+$), and 0.2 ($*$) (simulation sets A, B, and C).

Waite [2011], let k_m be the horizontal wavenumber of the local minimum of buoyancy flux seen in many of the transfer spectra in Figures 6, 7, 9, and define $L_m \equiv 2\pi/k_m$. This is the horizontal length scale where kinetic energy is injected by nonlinear interactions and partially converted to potential energy when Fr_h is sufficiently small and Re is sufficiently large. In Figure 8(a,b), L_m is plotted against the buoyancy and viscous scales for the simulations in which a clear bump in $B(k_h)$ could be identified. For the range of parameters considered here, L_m scales fairly well with both L_b and L_{visc}; a wider range of Re_b would possibly be able to distinguish between these two scalings. By contrast, L_m does not scale particularly well with either the Ozmidov or Kolmogorov scales (Figure 8c,d), which are both much smaller than L_m. *Waite* [2011] found $L_m \sim L_b$ in simulations with viscous effects reduced by hyperviscosity, which models the regime of effectively large Re_b. The small-scale injection of kinetic energy and associated spectral bumps therefore appear to be signatures of the vertical layer thickness in the horizontal spectrum. This connection between vertical and horizontal is consistent with the roll-up of thin layers of horizontal vorticity into more isotropic Kelvin–Helmholtz billows, as seen in Figure 5.

4. Discussion and Conclusions

The stratified turbulence simulated in these numerical experiments is surprisingly reminiscent of the picture painted by *Lilly* [1983], despite the significant advances in understanding that have occurred over the last three decades. Of course, the energy transfer in these simulations is predominantly downscale, and there is no evidence of *Lilly's* [1983] hypothesized inverse cascade. Nevertheless, the layerwise structure that he anticipated is clearly visible. The layer thickness scales like the viscous scale L_{visc}, but for laboratory parameters with $Re_b \sim O(1)$, the viscous scale is very close to the buoyancy scale L_b. As a result, the layers in these simulations, despite being coupled by vertical viscosity, are thin enough to yield $Fr_v \sim O(1)$ and, at least intermittently, Kelvin–Helmholtz instabilities at small scales. For the larger values of $Re_b \approx 2$, these instabilities appear to break down into even smaller-scale three-dimensional turbulence, as foreseen by *Lilly* [1983].

The turbulent statistics in these simulations are quite sensitive to changes in Fr_h and Re, and as *Brethouwer et al.* [2007] have argued, some of this sensitivity appears as a dependence on Re_b. In particular, the kinetic energy spectrum has a power law range with a slope that steepens with decreasing Re_b. For the range of parameters considered here,

the slope goes from around -3 to -5 as Re_b goes from 2 down to 0.2. These spectra are all steeper than *Lindborg's* [2006] proposed -5/3, which is to be expected at $O(1)$ values of Re_b, since vertical dissipation is non-negligible across all k_h. The very steep -5 spectrum at small Re_b has been observed in other simulations where the buoyancy scale is inside the vertical dissipation range (viscous or ad hoc), and appears to be the asymptotic behavior for $Re_b \to 0$ [*Laval et al.*, 2003; *Waite and Bartello*, 2004; *Brethouwer et al.*, 2007]. At small Re_b, the entire range of k_h is essentially a dissipation range for the vertical part of the viscous term; energy injected at large scales is dissipated at large scales, and no energy cascade to small horizontal scales occurs.

The dependence of the turbulent statistics on Re_b does not explain all of the sensitivity to Fr_h and Re observed in these simulations. In fact, there does seem to be some significant variability in the slope of the power law part of the spectrum, even at constant Re_b. For our largest Re_b values, the kinetic energy spectrum steepens as Fr_h decreases (with a corresponding increase in Re to keep $Re_b \approx 2$). The spectral slopes range from -2 to -3, and the steepening of these spectra has not quite converged, even for $Fr_h = 0.017$ and $Re = 9400$ – further steepening may therefore occur as Fr_h is decreased more. The size of the vertical dissipation, as approximated by Re_b^{-1} in (22), is therefore not the only parameter that determines the shape of the spectra, even at small Fr_h and large Re. It would be interesting to see if this behavior occurs at higher values of Re_b, and whether it yields spectra steeper than -5/3 for $Re_b \gg 1$.

Furthermore, many of these simulations exhibit spectral bumps at small horizontal scales, and the shape and position of these bumps are not solely determined by Re_b. These bumps appear to result from the injection of kinetic energy by nonlinear interactions, and their position scales like L_b and L_{visc} (it is not possible to distinguish between these scalings for $Re_b \sim O(1)$). Neither L_b nor L_{visc} is a simple function of Re_b alone, since

$$L_b \equiv 2\pi L_h \sqrt{\frac{Re_b}{Re}}, \quad L_{visc} \equiv 2\pi L_h \frac{1}{\sqrt{Re}}. \tag{30}$$

Both depend on Re in addition to Re_b, and both become smaller as Re is increased at fixed Re_b. *Waite* [2011] described spectral bumps with similar scaling in simulations that employed hyperviscosity to reduce viscous effects at large scales. In those simulations, a direct, non-local transfer of kinetic energy from large horizontal scales to L_b was found to be responsible for the bumps in the spectra. As in *Waite* [2011], the spectral bumps in the DNS in this chapter are consistent with Kelvin–Helmholtz instabilities transferring energy directly from large scales to the billow scale. For our largest $Re_b \approx 2$, the billows break down into smaller-scale turbulence and the peaks are broad; for smaller Re_b, the instabilities become more intermittent and seem to be

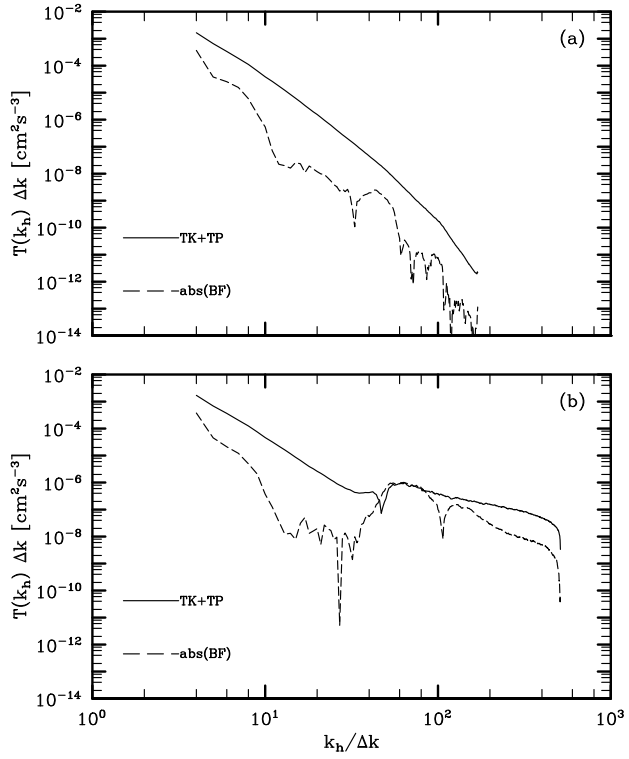

Figure 9. Horizontal wave number spectra of total energy transfer and buoyancy flux in simulations with fixed $Re_b \approx 0.2$ and different Fr_h and Re, corresponding to $Fr_h =$ (a) 0.0069 and (b) 0.0034 (runs C4 and C6). Log–log axes are used for clarity. As a result, only $k_h/\Delta k \geq 4$ are shown, and the absolute value of the buoyancy flux is taken. The buoyancy flux is positive over almost all k_h, but the peaks around $k_h/\Delta k \approx 40$ in (a) and 60 in (b) are negative.

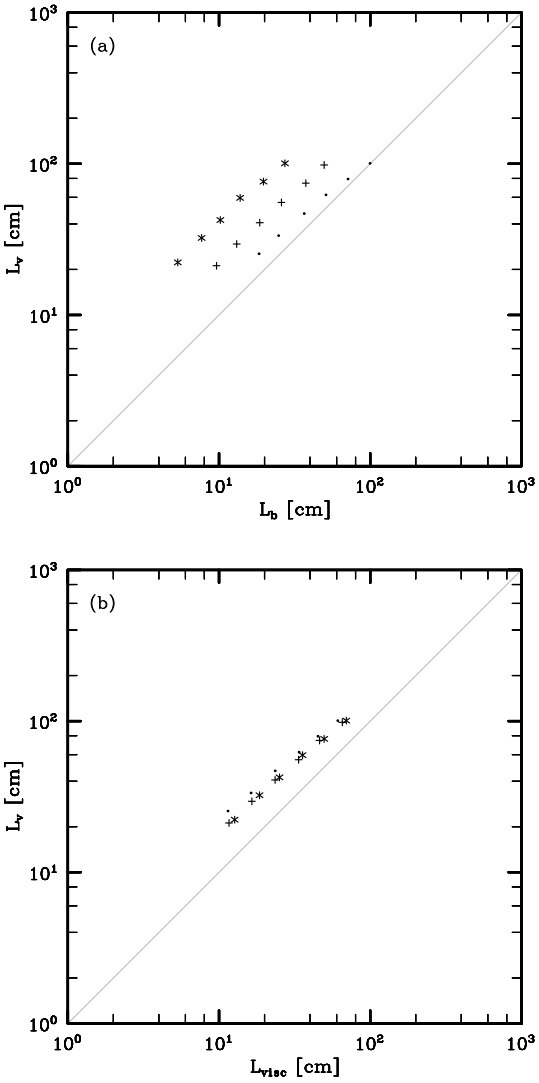

Figure 10. The characteristic vertical length scale L_v plotted against (a) the buoyancy scale L_b and (b) the viscous scale L_{visc}. Symbols denote $Re_b \approx 2$ ($\cdot$), 0.6 ($+$), and 0.2 ($*$) (simulation sets A, B, and C).

directly damped by viscosity, and the peaks are narrower. It is interesting that these small-scale transitions occur even for small $Re_b \approx 0.2$, at least for sufficiently large Re and small Fr_h. Even though the vertical Froude number based on mean quantities is smaller than 1, it is likely that there are intermittent patches of locally small Richardson number and subsequent instability as seen in Figure 5(c). Presumably, there is a threshold Re_b below which no instabilities occur for any Re and Fr_h, but these simulations show that such a cut-off value is less than 0.2.

Given the similarity between the simulations presented in this chapter and those of *Waite* [2011], it seems reasonable to speculate that the location of the spectral bumps seen here will scale with the buoyancy scale L_b in DNS with $Re_b \gg 1$. This scaling would suggest the existence of a distinct spectral range between the buoyancy scale, where kinetic energy in injected by instability of the large-scale flow, and the Ozmidov scale, where these instabilities ultimately break down into three-dimensional isotropic turbulence. However, reproducing this range requires large Re_b along with small Fr_h, and thus Reynolds numbers and numerical resolutions that are beyond the laboratory regime; *Bartello and Tobias* [2012] suggest $Re \gtrsim 10^5$, which is an order of magnitude larger than the highest Re values here. This range of scales between L_b and L_O is a key feature of geophysical stratified turbulence that is missing in laboratory-scale experiments and most numerical simulations because of the extremely high computational cost of resolving it. Indeed, typical values of L_b and L_O in the atmosphere are $O(1)$ km and $O(100)$ m, and so this scale range is not normally resolved in mesoscale simulations with $\Delta x \sim O(1)$ km. Interestingly, bumps in the atmospheric kinetic energy spectrum have been observed at this scale [e.g. *Vinnichenko*, 1970].

These DNS results underscore the care that must be taken when using laboratory-scale stratified turbulence as a proxy for the atmospheric mesoscale and oceanic sub-mesoscale. In particular, steep spectral slopes from experiments with $Re_b \sim O(1)$ should not be extrapolated too literally to geophysical scales. All else being equal, spectra do get shallower as Re_b increases, although it is still an open question whether the limiting slope for $Re_b \to \infty$ is -5/3 or something else. Nevertheless, it is quite encouraging that these simulations are able to capture some basic phenomena that are expected to hold at larger Re_b. In particular, the transfer of kinetic energy to small horizontal scales by Kelvin–Helmholtz instabilities appears to be quite robust, even for relatively modest values of Re_b, suggesting that the related spectral bumps (if not the subsequent turbulent breakdown) may be realizable in laboratory experiments.

A more serious concern about the geophysical applicability of idealized laboratory experiments and numerical simulations such as these is the question of how energy gets into the large scales to begin with. Simulations and experiments necessarily employ ad hoc methods to inject energy at large scales, either through initial conditions and/or forcing. But in the real atmosphere and ocean, the large-scale motion is not stratified turbulence at all, but rather quasi-geostrophic turbulence forced by radiative heating, surface fluxes, and baroclinic instability. The cascade through the atmospheric mesoscale and oceanic sub-mesoscale that is envisioned by the stratified turbulence hypothesis must be forced by the breakdown of this larger-scale motion, for which the effects of rotation cannot be ignored [e.g. *Bartello*, 2010; *Molemaker et al.*, 2010; *Vallgren et al.*, 2011]. The extent to which the influence of this large-scale motion extends down into the mesoscale/sub-mesoscale and beyond is still an open question that requires further study.

Acknowledgments. This work was supported by a grant from the Natural Sciences and Engineering Research Council of Canada. Computations were performed on the GPC supercomputer at the SciNet HPC Consortium [*Loken et al.*, 2010]. SciNet is funded by the Canada Foundation for Innovation under the auspices of Compute Canada, the Government of Ontario, Ontario Research Fund – Research Excellence, and the University of Toronto.

References

Almalkie, S., and S. M. deBruynKops (2012), Kinetic energy dynamics in forced, horizontally homogeneous and isotropic, stably stratified turbulence, *J. Turbul.*, *13*, N29.

Babin, A., A. Mahalov, B. Nicolaenko, and Y. Zhou (1997), On the asymptotic regimes and the strongly stratified limit of rotating Boussinesq equations, *Theor. Comput. Fluid Dyn.*, *9*, 223–251.

Bartello, P. (2000), Potential vorticity, resonance and dissipation in rotating convective turbulence, in *Geophysical and Astrophysical Convection*, edited by R. H. Kerr, P. Fox, and C.-H. Moeng, pp. 309–321.

Bartello, P. (2010), Quasigeostrophic and stratified turbulence in the atmosphere, in *IUTAN Symposium on Turbulence in the Atmosphere and Oceans*, vol. IUTAM Bookseries 28, edited by D. G. Dritschel, pp. 117–130, Springer.

Bartello, P., and S. Tobias (2012), Sensitivity of stratified turbulence to the buoyancy Reynolds number, *J. Fluid Mech.*, submitted.

Billant, P., and J.-M. Chomaz (2000), Three-dimensional stability of a vertical columnar vortex pair in a stratified fluid, *J. Fluid Mech.*, *419*, 65–91.

Billant, P., and J.-M. Chomaz (2001), Self-similarity of strongly stratified inviscid flows, *Phys. Fluids*, *13*, 1645–1651.

Brethouwer, G., P. Billant, E. Lindborg, and J.-M. Chomaz (2007), Scaling analysis and simulation of strongly stratified turbulent flows, *J. Fluid Mech.*, *585*, 343–368.

Charney, J. G. (1971), Geostrophic turbulence, *J. Atmos. Sci.*, *28*, 1087–1095.

Cho, J. Y. N., Y. Zhu, R. E. Newell, B. E. Anderson, J. D. Barrick, G. L. Gregory, G. W. Sachse, M. A. Carroll, and G. M. Albercook (1999), Horizontal wavenumber spectra of winds, temperature, and trace gases during the Pacific Exploratory Missions: 1. Climatology, *J. Geophys. Res.*, *104*, 5697–5716.

Dewan, E. M. (1979), Stratospheric wave spectra resembling turbulence, *Science*, *204*, 832–835.

Drazin, P. G. (1961), On the steady flow of a fluid of variable density past an obstacle, *Tellus*, *13*, 239–251.

Durran, D. R. (1999), *Numerical Methods for Wave Equations in Geophysical Fluid Dynamics*, Springer.

Embid, P. F., and A. J. Majda (1998), Low Froude number limiting dynamics for stably stratified flow with small or finite Rossby numbers, *Geophys. Astrophys. Fluid Dyn.*, *87*, 1–50.

Gage, K. S. (1979), Evidence for a $k^{-5/3}$ law inertial range in mesoscale two-dimensional turbulence, *J. Atmos. Sci.*, *36*, 1950–1954.

Gage, K. S., and G. D. Nastrom (1986), Theoretical interpretation of atmospheric wavenumber spectra of wind and temperature observed by commercial aircraft during GASP, *J. Atmos. Sci.*, *43*, 729–740.

Herring, J. R., and O. Métais (1989), Numerical experiments in forced stably stratified turbulence, *J. Fluid Mech.*, *202*, 97–115.

Hopfinger, E. J. (1987), Turbulence in stratified fluids: A review, *J. Geophys. Res.*, *92*, 5287–5303.

Kimura, Y., and J. R. Herring (2012), Energy spectra of stably stratified turbulence, *J. Fluid Mech.*, *698*, 19–50.

Kolmogorov, A. N. (1941), The local structure of turbulence in incompressible viscous fluid for very large Reynolds number, *Dok. Akad. Nauk. SSSR*, *30*, 301–305.

Kraichnan, R. H. (1967), Inertial ranges in two-dimensional turbulence, *Phys. Fluids*, *10*, 1417–1423.

Laval, J.-P., J. C. McWilliams, and B. Dubrulle (2003), Forced stratified turbulence: Successive transitions with Reynolds number, *Phys. Rev. E*, *68*, 036,308.

Lilly, D. K. (1983), Stratified turbulence and the mesoscale variability of the atmosphere, *J. Atmos. Sci.*, *40*, 749–761.

Lilly, D. K., G. Bassett, K. Droegemeier, and P. Bartello (1998), Stratified turbulence in the atmospheric mesoscale, *Theor. Comput. Fluid Dyn.*, *11*, 139–153.

Lin, J. T., and Y. H. Pao (1979), Wakes in stratified fluids: A review, *Annu. Rev. Fluid Mech.*, *11*, 317–338.

Lindborg, E. (2006), The energy cascade in a strongly stratified fluid, *J. Fluid Mech.*, *550*, 207–242.

Lindborg, E., and J. Y. N. Cho (2001), Horizontal velocity structure functions in the upper troposphere and lower stratosphere. 2. Theoretical considerations, *J. Geophys. Res.*, pp. 10,233–10,241.

Loken, C., et al. (2010), SciNet: Lessons learned from building a power-efficient top-20 system and data centre, *J. Phys.: Conf. Ser.*, *256*, 012,026.

Lumley, J. L. (1964), The spectrum of nearly inertial turbulence in a stably stratified fluid, *J. Atmos. Sci.*, *21*, 99–102.

Moin, P., and K. Mahesh (1998), Direct numerical simulation: A tool in turbulence research, *Annu. Rev. Fluid Mech.*, *30*, 539–578.

Molemaker, M. J., J. C. McWilliams, and X. Capet (2010), Balanced and unbalanced routes to dissipation in an equilibrated eady flow, *J. Fluid Mech.*, *654*, 35–63.

Munk, W. (1981), Internal waves and small-scale processes, in *Evolution of Physical Oceanography*, edited by B. A. Warren and C. Wunsch, pp. 264–291.

Nastrom, G. D., and K. S. Gage (1985), A climatology of atmospheric wavenumber spectra observed by commercial aircraft, *J. Atmos. Sci.*, *42*, 950–960.

Ozmidov, R. V. (1965), On the turbulent exchange in a stably stratified ocean, *Izvestia Akad. Nauk. SSSR Atmospheric and Oceanic Physics Ser.*, *1*, 853–860.

Praud, O., A. M. Fincham, and J. Sommeria (2005), Decaying grid turbulence in a strongly stratified fluid, *J. Fluid Mech.*, *522*, 1–33.

Riley, J. J., and S. M. deBruynKops (2003), Dynamics of turbulence strongly influenced by buoyancy, *Phys. Fluids*, *15*, 2047–2059.

Riley, J. J., and M.-P. Lelong (2000), Fluid motions in the presence of strong stable stratification, *Annu. Rev. Fluid Mech.*, *32*, 613–657.

Riley, J. J., and E. Lindborg (2008), Stratified turbulence: A possible interpretation of some geophysical turbulence measurements, *J. Atmos. Sci.*, *65*, 2416–2424.

Riley, J. J., R. W. Metcalfe, and M. A. Weissman (1981), Direct numerical simulations of homogeneous turbulence in density-stratified fluids, in *Nonlinear Properties of Internal Waves*, edited by B. J. West, pp. 79–112.

Smith, L. M., and F. Waleffe (2002), Generation of slow large scales in forced rotating stratified turbulence, *J. Fluid Mech.*, *451*, 145–168.

Smyth, W. D., and J. N. Moum (2000), Anisotropy of turbulence in stably stratified mixing layers, *Phys. Fluids*, *12*, 1343–1362.

Staquet, C., and J. Sommeria (2002), Internal gravity waves: From instabilities to turbulence, *Annu. Rev. Fluid Mech.*, *34*, 559–593.

Sullivan, N. P., S. Mahalingam, and R. M. Kerr (1994), Deterministic forcing of homogeneous, isotropic turbulence, *Phys. Fluids*, *6*, 1612–1614.

Tulloch, R., and K. S. Smith (2009), Quasigeostrophic turbulence with explicit surface dynamics: Application to the atmospheric energy spectrum, *J. Atmos. Sci.*, *66*, 450–467.

Tung, K. K., and W. W. Orlando (2003), The k^{-3} and $k^{-5/3}$ energy spectrum of atmospheric turbulence: Quasigeostrophic two-level model simulation, *J. Atmos. Sci.*, *60*, 824–835.

Vallgren, A., E. Deusebio, and E. Lindborg (2011), Possible explanations of the atmospheric kinetic and potential energy spectra, *Phys. Rev. Lett.*, *107*, 268501.

VanZandt, T. E. (1982), A universal spectrum of buoyancy waves in the atmosphere, *Geophys. Res. Lett.*, *9*, 575–578.

Vinnichenko, N. K. (1970), The kinetic energy spectrum in the free atmosphere – 1 second to 5 years, *Tellus*, *22*, 158–166.

Waite, M. L. (2011), Stratified turbulence at the buoyancy scale, *Phys. Fluids*, *23*, 066,602.

Waite, M. L., and P. Bartello (2004), Stratified turbulence dominated by vortical motion, *J. Fluid Mech.*, *517*, 281–308.

Waite, M. L., and P. Bartello (2006), Stratified turbulence generated by internal gravity waves, *J. Fluid Mech.*, *546*, 313–339.

Waite, M. L., and C. Snyder (2013), Mesoscale energy spectra of moist baroclinic waves, *J. Atmos. Sci.*, in press.

M. L. Waite, Department of Applied Mathematics, University of Waterloo, 200 University Avenue West, Waterloo, Ontario, N2L 3G1, Canada. (mwaite@uwaterloo.ca)